A Gain-of-Function Mutation of Arabidopsis CRYPTOCHROME1 Promotes Flowering[1][W][OA]

Vivien Exner, Cristina Alexandre, Gesa Rosenfeldt, Pietro Alfarano, Mena Nater, Amedeo Caflisch, Wilhelm Gruissem, Alfred Batschauer, and Lars Hennig*

Department of Biology and Zurich-Basel Plant Science Center, Eidgenössisch Technische Hochschule Zurich, 8129 Zurich, Switzerland (V.E., C.A., M.N., W.G., L.H.); Fachbereich Biologie/Pflanzenphysiologie, Philipps-Universität, 35032 Marburg, Germany (G.R., A.B.); Department of Biochemistry, University of Zurich, 8057 Zurich, Switzerland (P.A., A.C.); and Department of Plant Biology and Forest Genetics, Uppsala BioCenter, Swedish University of Agricultural Sciences, 75007 Uppsala, Sweden (L.H.)

Plants use different classes of photoreceptors to collect information about their light environment. Cryptochromes are blue light photoreceptors that control deetiolation, entrain the circadian clock, and are involved in flowering time control. Here, we describe the *cry1-L407F* allele of Arabidopsis (*Arabidopsis thaliana*), which encodes a hypersensitive cryptochrome1 (cry1) protein. Plants carrying the *cry1-L407F* point mutation have elevated expression of *CONSTANS* and *FLOWERING LOCUS T* under short-day conditions, leading to very early flowering. These results demonstrate that not only the well-studied cry2, with an unequivocal role in flowering promotion, but also cry1 can function as an activator of the floral transition. The *cry1-L407F* mutants are also hypersensitive toward blue, red, and far-red light in hypocotyl growth inhibition. In addition, *cry1-L407F* seeds are hypersensitive to germination-inducing red light pulses, but the far-red reversibility of this response is not compromised. This demonstrates that the cry1-L407F photoreceptor can increase the sensitivity of phytochrome signaling cascades. Molecular dynamics simulation of wild-type and mutant cry1 proteins indicated that the L407F mutation considerably reduces the structural flexibility of two solvent-exposed regions of the protein, suggesting that the hypersensitivity might result from a reduced entropic penalty of binding events during downstream signal transduction. Other nonmutually exclusive potential reasons for the *cry1-L407F* gain of function are the location of phenylalanine-407 close to three conserved tryptophans, which could change cry1's photochemical properties, and stabilization of ATP binding, which could extend the lifetime of the signaling state of cry1.

Light determines the plant's life, because light is the essential energy source for plant metabolism. The spatial, temporal, and spectral variability of light provides cues about the time of day, the season, and the presence of competitors for light. Sensitive and precise light perception, therefore, is essential to properly adjust plant development for maximal photosynthetic efficiency, to correlate vegetative and reproductive growth with favorable seasons, and eventually to maximize fitness. To cope with this task, plants have evolved several types of photoreceptors, including the phytochromes and cryptochromes (for review, see Banerjee and Batschauer, 2005; Josse et al., 2008; Müller and Carell, 2009). Phytochromes are red and far-red light receptors and regulate different aspects of plant development, such as hypocotyl elongation in red and far-red light and shade avoidance responses (Franklin et al., 2005). In addition, the two major phytochromes in Arabidopsis (*Arabidopsis thaliana*), phytochrome A (phyA) and phyB, are involved in flowering time control: phyA promotes flowering under short-day (SD) and long-day (LD) photoperiods (Johnson et al., 1994), while phyB acts as a floral inhibitor (Reed et al., 1993; Mockler et al., 1999).

Cryptochromes are flavoproteins with two chromophores that sense blue and UV-A light in plants (Lin and Todo, 2005). The essential chromophore is a FAD, and the second chromophore is supposed to function in light harvesting and is a pterine (methenyltetrahydrofolate; Müller and Carell, 2009). Cryptochromes have an N-terminal photolyase-related (PHR) domain that is similar to photolyases, but they are distinguished from the latter by a variable C-terminal domain. Furthermore, crystallization of the photolyase-like domain of Arabidopsis cryptochrome1 (cry1) has revealed additional structural differences between photolyase and cryptochrome that explain the lack of DNA-binding activity of the cryptochromes (Brautigam et al., 2004). Moreover, the crystal structure confirmed the previ-

[1] This work was supported by the Swiss National Science Foundation (grant no. 3100AO–116060 to L.H.), by Eidgenössisch Technische Hochschule Zurich (project no. TH–16/05–2 to L.H.), and by the Deutsch Forschungsgemeinschaft (grant no. BA985/11–1 to A.B.).

* Corresponding author; e-mail lars.hennig@vbsg.slu.se.

The author responsible for distribution of materials integral to the findings presented in this article in accordance with the policy described in the Instructions for Authors (www.plantphysiol.org) is: Lars Hennig (lars.hennig@vbsg.slu.se).

[W] The online version of this article contains Web-only data.

[OA] Open Access articles can be viewed online without a subscription.

www.plantphysiol.org/cgi/doi/10.1104/pp.110.160895

ously described ATP binding of cry1 (Bouly et al., 2003) by soaking cry1 crystals with the nonhydrolyzable ATP analog adenosine 5′-[β,γ-imido]triphosphate (AMP-PNP) and showing AMP-PNP located in the FAD access cavity (Brautigam et al., 2004). Despite the available protein structure, cryptochrome's mode of action still remains to be determined. Interestingly, the C terminus of plant cryptochromes as well as a C-terminal 80-residue motif (NC80) confer constitutive cryptochrome signaling when overexpressed in plants even in the absence of light (Yang et al., 2000; Yu et al., 2007). For plant cryptochromes, it has been proposed that the PHR domain and the C terminus form a "closed" conformation to mask the NC80 motif in the absence of light. Blue light would trigger phosphorylation of the C-terminal tail and its electrostatic repulsion from the surface of the PHR domain to form an "open" conformation, exposing the NC80 motif and initiating signal transduction (Yu et al., 2007).

The Arabidopsis genome harbors two cryptochrome genes: *CRY1* and *CRY2*. A third member of this family, *CRY3*, belongs to the DASH-type subgroup with repair activity for cyclobutane pyrimidine dimer lesions in single-stranded DNA (Selby and Sancar, 2006) and loop structures of duplex DNA (Pokorny et al., 2008), but with so far unproven photoreceptor function. Mutations in both *CRY1* and *CRY2* interfere with the inhibition of hypocotyl elongation under blue light conditions (Ahmad and Cashmore, 1993; Guo et al., 1998). Current data suggest that cry1 is the major blue light receptor for seedling photomorphogenesis, while cry2 is more important for the control of flowering time (Guo et al., 1998; Mockler et al., 1999, 2003; El-Din El-Assal et al., 2003; Endo et al., 2007). Nevertheless, several studies also reported cry1 as a floral regulator: some *cry1* mutant alleles conferred late flowering under certain growth conditions (Bagnall et al., 1996; Blázquez et al., 2003), but others did not (Zagotta et al., 1996; Mockler et al., 1999).

Even though the functions of the different photoreceptors are assigned to specific segments of the spectrum of light, physiological and mutant analyses have revealed extensive cross talk between blue and red light photoreceptors (Casal, 2000): phyA and phyB display antagonistic and synergistic effects on the action of each other, depending on which responses are studied (Reed et al., 1994; Casal and Boccalandro, 1995), and several of the phytochromes functionally interact with the cryptochromes (Ahmad and Cashmore, 1997; Casal and Mazzella, 1998; Neff and Chory, 1998; Hennig et al., 1999; Mockler et al., 1999; Devlin and Kay, 2000). In addition, a physical interaction of phyA with cry1 (Ahmad et al., 1998b) and of phyB with cry2 (Más et al., 2000) has been reported. While these cross talks are of minor importance under controlled monochromatic light conditions, they are probably essential for fine-tuning of developmental programs in natural environments.

Here, we provide evidence that a hyperactive *cry1* allele confers hypersensitivity not only to blue light but also to red light and strongly shortens flowering time under SD.

RESULTS

Isolation of a New *cry1* Allele

For a suppressor screen, seeds of the late-flowering *msi1-tap1* transgenic line (Bouveret et al., 2006) were mutagenized with ethyl methane sulfonate (EMS; Exner et al., 2009). Flowering time was scored under LD photoperiods for 1,045 M2 families. Among these, 11 families segregated plants that shortened the vegetative phase of *msi1-tap1*. For six of them, we confirmed the phenotype in subsequent generations. One of these six contained a mutation in *LIKE HETEROCHROMATIN PROTEIN1* (Exner et al., 2009); the others belong to at least four complementation groups (data not shown). All these mutants still reacted to changes in daylength but exhibited different responses as tested by flowering time experiments under LD and SD (data not shown). The mutant with ID 0.3-457 was chosen for further characterization (Table I).

The mutation in 0.3-457 was localized between markers CER446440 (bacterial artificial chromosome T3H13) and CER460528 (bacterial artificial chromosome T3H13) on the lower arm of chromosome IV. This region contains nine genes including *CRY1*. Sequencing of the *CRY1* locus revealed a C-to-T transition in the third exon, 1,469 bp after the ATG start codon (Fig. 1A), which caused a change of Leu-407 to Phe (Fig. 1B). Therefore, 0.3-457 is henceforth called *cry1-L407F*.

Comparison of cryptochrome and photolyase sequences from different organisms revealed that Leu-407, which is located in the photolyase-like PHR domain, is conserved among nearly all plant cryptochromes. Among the few exceptions are Arabidopsis, *Arabidopsis lyrata* and *Fragaria vesca* (strawberry) CRY2, which all have an Ile instead of the Leu at this position (Fig. 1B). In contrast, photolyases and animal cryptochromes have amino acids with small side chains (Ala, Ser, Thr, or Gly) at this position but rarely if ever a bulky hydrophobic residue such as Leu. We did not find any cryptochrome or photolyase sequence with a Phe at this position. Furthermore, Leu-407 is located in a block of 12 amino acids that are highly conserved in plant cryptochromes but not in photolyases and animal cryptochromes. A structure of the cry1 PHR domain has been reported (Brautigam et al., 2004), and

Table I. *Flowering time of 03-457*

Values shown are means ± SE ($n \geq 10$). Note that 0.3-457 was in the *msi1-tap1* background.

Genotype	Flowering Time in LD	Flowering Time in SD
	d	
Col	23.9 ± 0.6	81.8 ± 1.8
msi1-tap1	38.5 ± 1.2	117.9 ± 6.1
0.3-457	28.4 ± 0.3	51.4 ± 1.7

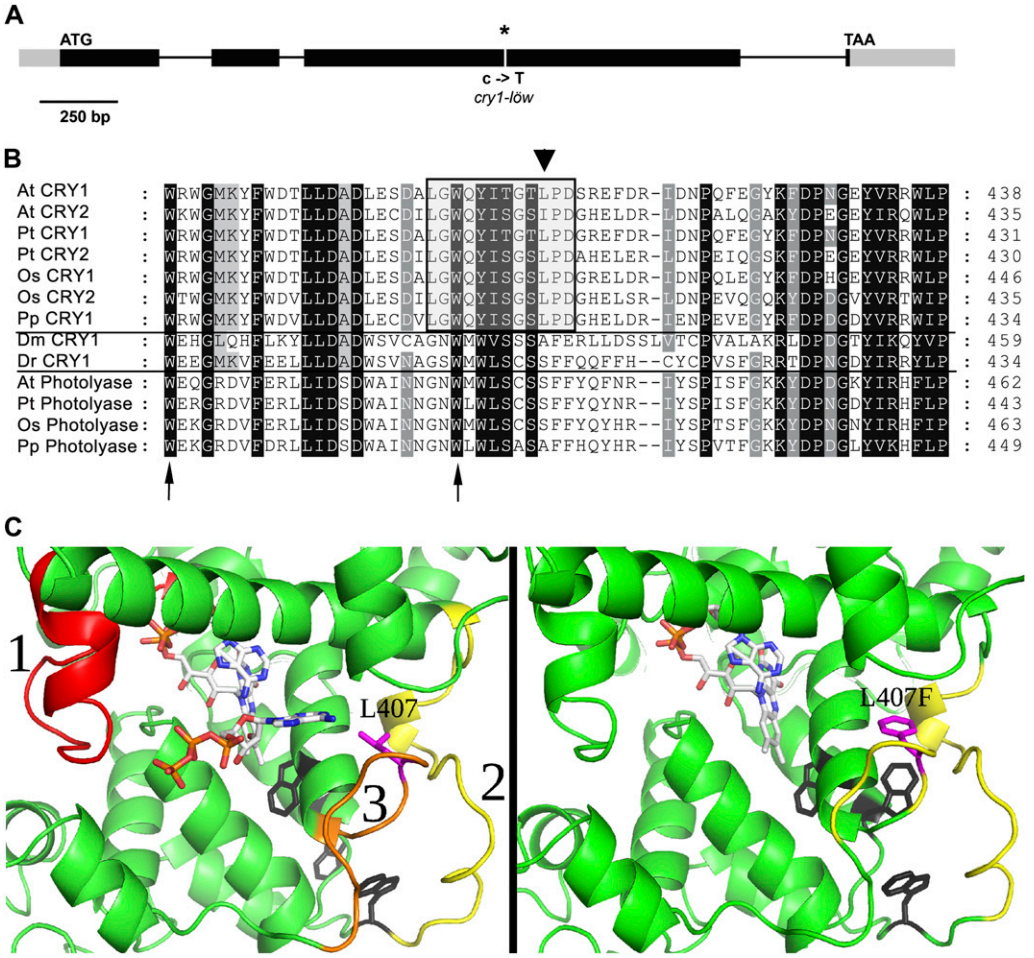

Figure 1. CRY1 sequence context of the conserved Leu-407. A, Structure of the Arabidopsis *CRY1* gene. Boxes represent exons; positions of translational start and stop as well as of the L407F mutation are shown; gray boxes represent untranslated regions. B, Cryptochrome and photolyase protein sequences of several organisms were aligned, and a segment of the generated sequence alignment is shown; numbers at the end of each line indicate the amino acid position within the respective protein. The arrowhead marks the Leu that is exchanged for a Phe in CRY1-L407F. Note that this Leu is usually conserved in plant cryptochromes but not in photolyases. The arrows indicate conserved Trp residues involved in electron transfer to FAD. The gray box marks a plant cryptochrome-specific 12-amino acid motif that includes Leu-407. C, Left, x-ray structure of the complex of cry1, FAD, and ATP taken from Brautigam et al. (2004). Conserved Trp residues are in black, and Leu-407 is in magenta. The red, yellow, and orange sequence regions (labeled 1, 2, and 3, respectively) correspond to the peaks in the RMSF plot (see text). Right, structural model of cry1-L407F. The mutation L407F is in magenta. The first 20 residues, for which the reduction of flexibility caused by the L407F mutation is highest, are in yellow.

according to this structure, Leu-407 is buried inside the protein without solvent contact (Fig. 1C).

cry1-L407F Strongly Accelerates Flowering

The *cry1-L407F* mutant did not only flower earlier in the *msi1-tap1* background but also when backcrossed into the Columbia (Col) wild type both under LD and SD conditions (Fig. 2, A and B). Under LD, the acceleration of flowering in *cry1-L407F* was caused by a shortened adult phase (0.8 versus 2.6 leaves), while the duration of the juvenile phase (5.3 leaves) was not affected. The early-flowering phenotype was even more dramatic under SD. While wild-type plants produced 61 leaves before bolting, *cry1-L407F* produced only 12 leaves. Tests for genetic interaction between *cry1-L407F* and *msi1-tap1* revealed additivity of both mutants (Supplemental Fig. S1), suggesting that *CRY1* and *MSI1* function in separate genetic pathways in the control of flowering. Besides the early-flowering phenotype, *cry1-L407F* featured a small and compact rosette (Supplemental Fig. S1), which is partly caused by shortened petioles (data not shown). Such a reduction of petiole length has also been described for plants overexpressing cry1 (Lin et al., 1996).

These results, together with the observation that *cry1-L407F* behaved semidominantly (data not shown), suggested that we identified a gain-of-function *CRY1* allele. Because genetic complementation tests and transgenic complementation are difficult with hypermorphic

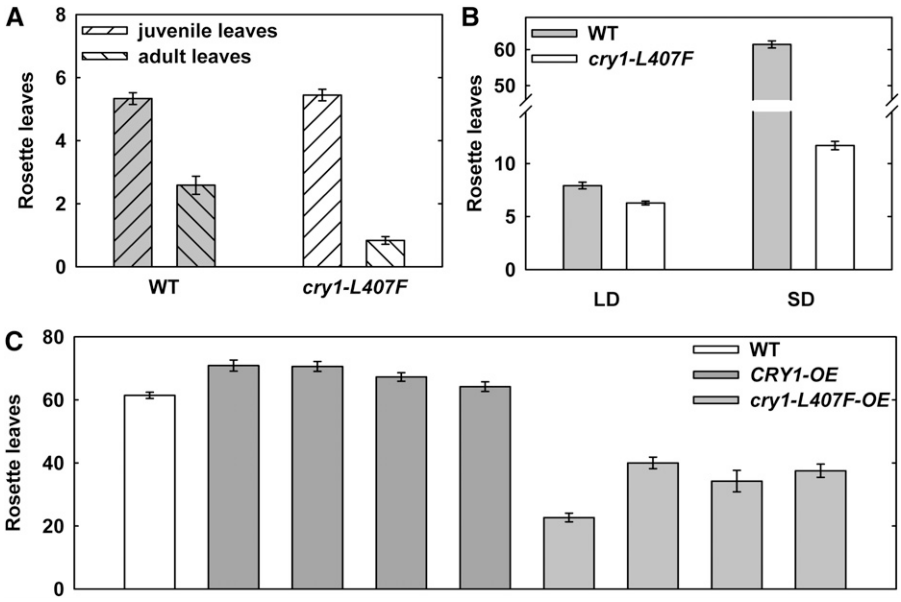

Figure 2. cry1-L407F mediates early flowering. A, Juvenile-adult phase transition of Col wild-type (WT) and *cry1-L407F* plants under LD photoperiods. B, Flowering time of Col wild-type and *cry1-L407F* plants under LD and SD photoperiods. C, Flowering time of wild-type plants and four randomly selected transgenic cry1- or cry1-L407F-overexpressing lines (OE) under SD photoperiods. Diagrams show means ± SE ($n \geq 14$).

and neomorphic alleles, the ability of cry1-L407F to accelerate flowering was tested by transgenic phenocopy experiments. When wild-type cry1 was introduced and overexpressed in Col wild-type plants, the four tested transgenic lines all flowered as late as or even slightly later than the Col wild type under SD (Fig. 2C). Similarly, Lin et al. (1996) had previously reported that increased cry1 dosage caused slightly delayed flowering. In contrast, when the *cry1-L407F* mutant gene under the control of the same cauliflower mosaic virus 35S promoter was introduced into Col, the four tested transgenic lines all flowered earlier than the Col wild type under SD (Fig. 2C).

Together, these results show that *cry1-L407F* is a gain-of-function *CRY1* allele that strongly accelerates flowering.

cry1-L407F Causes *FLOWERING LOCUS T* Overexpression

Cryptochromes can affect flowering in at least three different ways. First, cryptochromes control the phase of the circadian clock, which in turn controls diurnal expression patterns of *CONSTANS* (*CO*). Second, cryptochromes stabilize CO protein in the light, and CO then activates flowering by inducing the expression of *FLOWERING LOCUS T* (*FT*), which encodes the mobile flowering signal FT (for review, see Kobayashi and Weigel, 2007). Third, cry2 can directly induce *FT* expression (Liu et al., 2008a). To elucidate whether one of these mechanisms is involved in the accelerated flowering of *cry1-L407F*, we measured the gene expression of *EARLY FLOWERING4* (*ELF4*), *GIGANTEA* (*GI*), *CO*, and *FT* under SD conditions. ELF4 and GI participate in signaling from the circadian clock to downstream processes such as *CO* expression (Park et al., 1999; Doyle et al., 2002). In SD, *CO* is usually expressed only after the end of the light phase, and because CO protein is rapidly degraded in the dark, *FT* remains inactive. We found that *ELF4* expression was not significantly affected in *cry1-L407F*, maintaining its typical evening peak (Fig. 3), suggesting that the accelerated flowering was not caused by a malfunction of the circadian clock. Likewise, GI expression was very similar between the wild type and *cry1-L407F* (Fig. 3). In contrast, expression of *CO* and *FT* was considerably increased in *cry1-L407F* (Fig. 3). However, *FT* expression was strongest during the light period (zeitgeber time = 3 h), while *CO* expression was strongest during the dark period (zeitgeber time = 14 h), suggesting that cry1-L407F does not establish aberrant CO protein stabilization in the dark.

Together, these results indicate that cry1-L407F causes the untimely expression of *CO* during the light period and thus allows for the accumulation of CO under SD photoperiods. Increased CO levels then strongly activate *FT* and cause the very early flowering of wild-type plants and the suppression of *msi1-tap1*'s late-flowering phenotype.

cry1-L407F Causes Hypersensitivity toward Blue and Red Light

The cry1 photoreceptor is known to control hypocotyl growth in response to blue light (Koornneef et al., 1980; Ahmad and Cashmore, 1993). To investigate the effects of the amino acid substitution on the function of cry1-L407F in further detail, seedlings were grown under different fluence rates of blue, red, and far-red light and hypocotyl elongation was measured. Under blue light, inhibition of hypocotyl elongation was observed under much lower fluence rates in *cry1-L407F* than in the wild type (Fig. 4). Thus, cry1-L407F is a hypersensitive blue light photoreceptor, and *cry1-L407F* is a hypermorphic allele. The hypersensitivity of *cry1-L407F* toward blue light is a dominant trait.

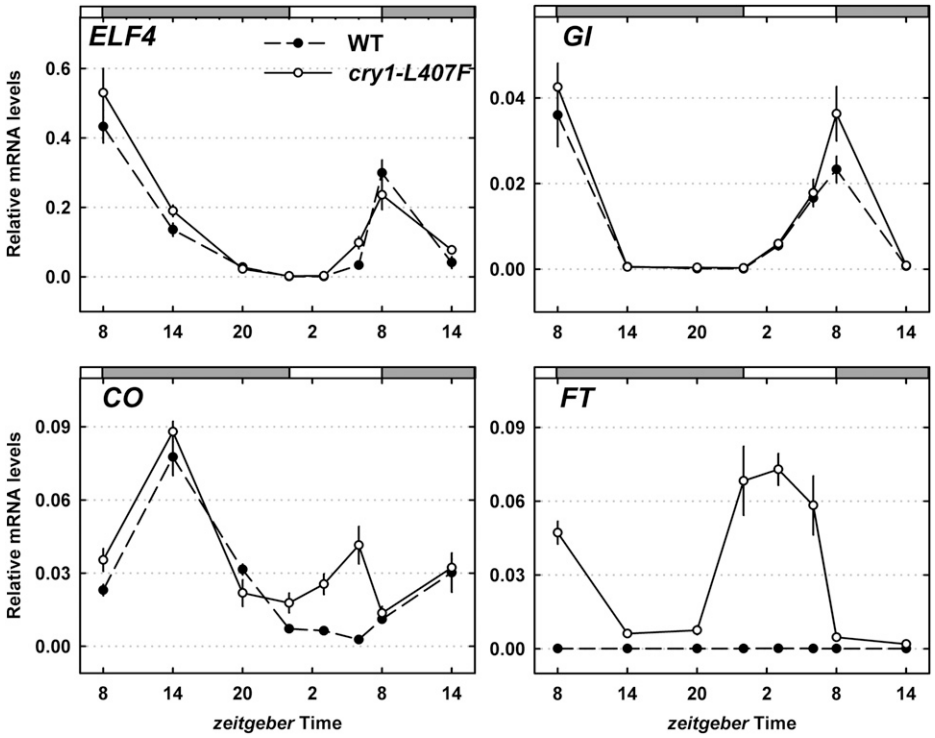

Figure 3. *CO* and *FT* transcript levels are increased in the *cry1-L407F* mutant. Quantitative RT-PCR was performed on cDNA from 15-d-old seedlings grown under SD conditions. Relative expression values are shown as mean ± SE ($n \geq 4$). White and gray bars on top of the diagrams represent periods of light and darkness, respectively. Values were normalized to a *PP2A* gene (At1g13320). WT, Wild type.

Heterozygous *cry1-L407F* seedlings uniformly displayed short hypocotyls when grown under low fluence rates of blue light (data not shown). Surprisingly, *cry1-L407F* seedlings were not only strongly hypersensitive to blue light but also to red light (Fig. 4), which should not efficiently activate cry1 (Lin et al., 1995; Ahmad et al., 2002). It is unlikely that this phenotype was caused by a "contamination" of the red light by photons from the blue part of the spectrum, because there is extremely little if any blue light emitted by the light source used in these experiments (Supplemental Fig. S2). Similar to the situation under red light, *cry1-L407F* seedlings were also hypersensitive to far-red light, which is believed to be predominantly sensed by phyA.

Repression of hypocotyl elongation under blue light is a normal function of wild-type Arabidopsis cry1 and cry2 (Koornneef et al., 1980; Ahmad and Cashmore, 1993; Lin et al., 1998). In order to test whether cry1-L407F does also affect the red light sensitivity of a process normally not controlled by cryptochromes, we compared light-dependent germination of the wild type and *cry1-L407F*. It is commonly thought that germination of Arabidopsis seeds is exclusively controlled by phytochromes but not by cryptochromes (Shinomura et al., 1996; Oh et al., 2007). Under continuous white light, both the wild type and *cry1-L407F* show a similarly high frequency of germination, while in the dark or after a far-red pulse, almost no germination occurred (Fig. 5). Pulses of red or white light that caused a germination rate of about 30% in wild-type seeds caused a germination rate of 80% in *cry1-L407F* seeds. Thus, cry1-L407F strongly increased the sensitivity of red light-induced germination. Red light-induced germination is usually a function of phyB. However, the results shown in Figure 5 could indicate that *cry1-L407F* itself can induce germination. Because photoreversibility is a hallmark of phyB function, we tested whether the red light-induced induction of germination could be reverted by a pulse of far-red light. Indeed, a far-red light pulse could completely prevent red light-induced germination in both the wild type and *cry1-L407F* (Fig. 5). This strongly suggests that cry1-L407F can increase the sensitivity to red light or signaling of photoreversible phytochromes such as phyB in the low fluence response.

The development of *cry1-L407F* seedlings differed from the wild type not only in the light but also in the dark. For up to 3 d of growth in the dark, hypocotyls were of similar length and cotyledons were folded into a protective hook in Col and *cry1-L407F*. In *cry1-L407F*, cotyledons started to unfold from day 2 on, and hypocotyl elongation was slightly reduced from day 3 on (Fig. 4; Supplemental Table S1; Supplemental Fig. S3). In addition, hypocotyls of dark-grown *cry1-L407F* were often bent while hypocotyls of the wild type grew straight (Supplemental Table S1; Supplemental Fig. S3). The hypocotyl-bending phenotype was temperature dependent: growth at 21°C led to strong bending in most of the seedlings, but growth at 26°C led to only mild bending (Supplemental Fig. S3). Thus, cry1-L407F can at least partially function even without light activation. Nevertheless, no strong constitutive activation of photomorphogenesis in the dark, such as was observed in plants overexpressing the CCT domain (Yang et al., 2000), was observed in *cry1-L407F*. For

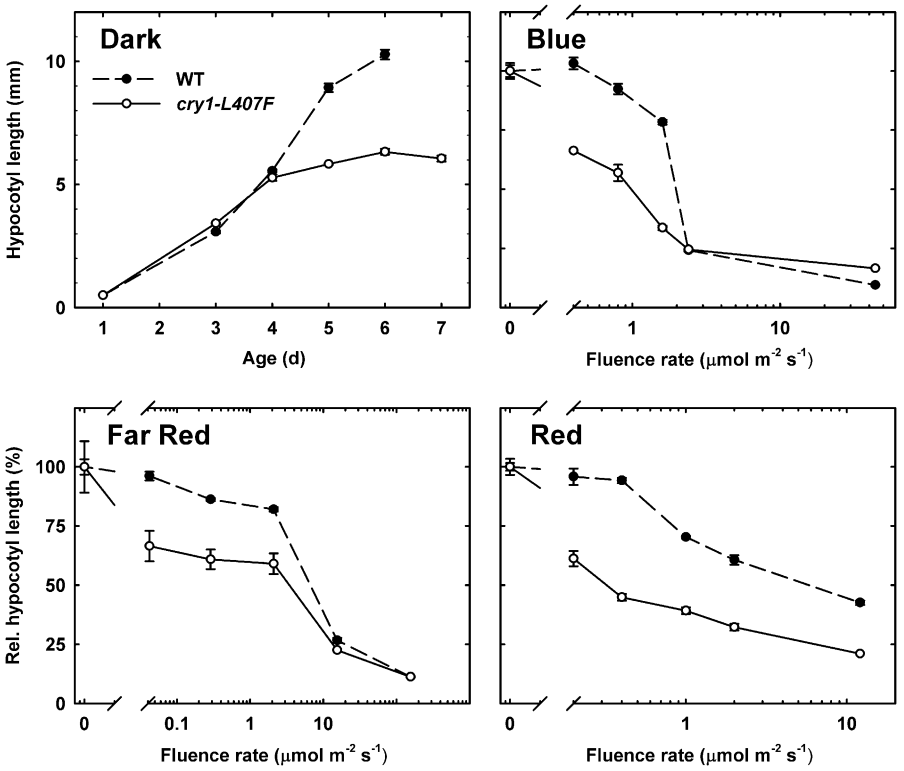

Figure 4. Inhibition of hypocotyl elongation in *cry1-L407F* mutant seedlings is hypersensitive to blue, red, and far-red light. Fluence rate response curves of hypocotyl growth inhibition under continuous light treatments are shown. Diagrams show means ± SE of three replicates with at least 15 seedlings analyzed in each experiment. Black circles, the wild type (WT); white circles, *cry1-L407F*.

example, there was no induction of cell division in the shoot apical meristem in the dark (data not shown).

Phytochromes regulate the transcription of many genes; *EARLY LIGHT INDUCED2* (*ELIP2*), for instance, is rapidly up-regulated after exposure to red or far-red light, and this up-regulation requires phyB and phyA, respectively (Harari-Steinberg et al., 2001). We tested whether the *cry1-L407F* mutation would affect the red light-induced expression of *ELIP2*. In darkness and during the investigated time course up to 6 h after transfer to red light, ELIP2 expression was consistently higher in *cry1-L407F* than in the wild type, but with very similar kinetics for both genotypes (Fig. 6). Thus, the effect of cry1-L407F on red light signaling is not restricted to germination and hypocotyl growth inhibition.

Together, these results show that *cry1-L407F* causes strong hypersensitivity to both blue and red light in a dominant manner.

The Hypersensitivity of *cry1-L407F* Is Not Caused by Elevated cry1 Levels

Overexpression of *CRY1* under the control of the constitutive 35S promoter results in hypersensitivity of the transgenic plants toward blue light (Lin et al.,

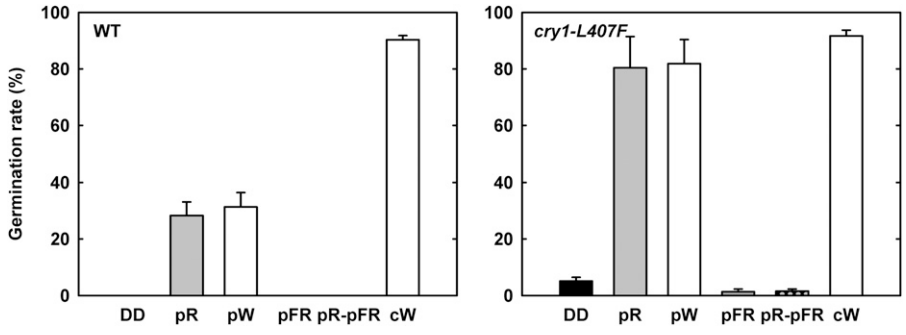

Figure 5. Induction of germination in *cry1-L407F* mutants is hypersensitive to white and red light. Seeds were sown under green light, stratified for 2 d at 4°C, and treated with light pulses. After 4 d in the dark, germination rates were determined. DD, No light treatment; pR, 30 min of red light (10.5 μmol m^{-2} s^{-1}); pW, 30 min of white light (130 μmol m^{-2} s^{-1}); pFR, 30 min of far-red light (110 μmol m^{-2} s^{-1}); pR-pFR, red pulse followed by far-red pulse; cW, continuous white light for 4 d (130 μmol m^{-2} s^{-1}); WT, wild type. Values shown are means ± SE of four replicate experiments with three different seed batches.

1996). Thus, we reasoned that the observed hypersensitivity of the *cry1-L407F* mutant could be caused by increased cry1 protein levels, although flowering time was not affected in overexpressors of wild-type cry1 (Fig. 2). Quantitative immunoblots, however, revealed unchanged cry1 levels in *cry1-L407F* mutants (Fig. 7; data not shown). These results demonstrate that the blue and red light hypersensitivity and early flowering of *cry1-L407F* are not caused by increased expression of cry1 but most likely by increased activity of the cry1-L407F protein. This conclusion is supported by the observation that blue fluence rates of up to 50 μmol m^{-2} s^{-1} caused a stronger shift of the cry1 band in the *cry1-L497F* mutant than in the wild type (Fig. 7). This blue light-induced shift reflects phosphorylation of the cry1 protein that is associated with photoreceptor activation (Shalitin et al., 2002, 2003; Bouly et al., 2003). We thus conclude that the L407F mutation in cry1 increases the fraction of active (phosphorylated) photoreceptor over a broad range of blue fluence rates but has no effect in darkness, as seen from the absence of a shifted cry1 band in both the wild type and the *cry1-L407F* mutant (Fig. 7).

The Hypersensitivity of *cry1-L407F* Could Be Caused by Reduced Structural Flexibility of the Photoreceptor

To understand the potential consequences of the L407F mutation on cry1 structure and function, we carried out three independent molecular dynamics simulations for each of the four following systems: wild-type protein and the L407F mutant, both with ATP and without ATP. The time series of root mean square deviation (RMSD) are useful to visualize the spatial deviation of the structure during the simulation with respect to the energy-minimized x-ray conformation (Supplemental Fig. S4). RMSD plots of the Cα atoms show that wild-type and mutant protein are

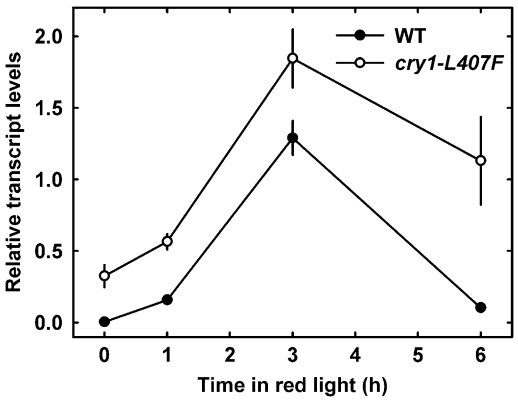

Figure 6. Induction of *ELIP2* expression in *cry1-L407F* mutants is hypersensitive to red light. Seedlings were grown for 4 d in the dark before being transferred to continuous red light (10.5 μmol m^{-2} s^{-1}). Relative expression values based on quantitative RT-PCR are shown as means ± SE ($n \geq 3$). Values were normalized to a *PP2A* gene (At1g13320). WT, Wild type.

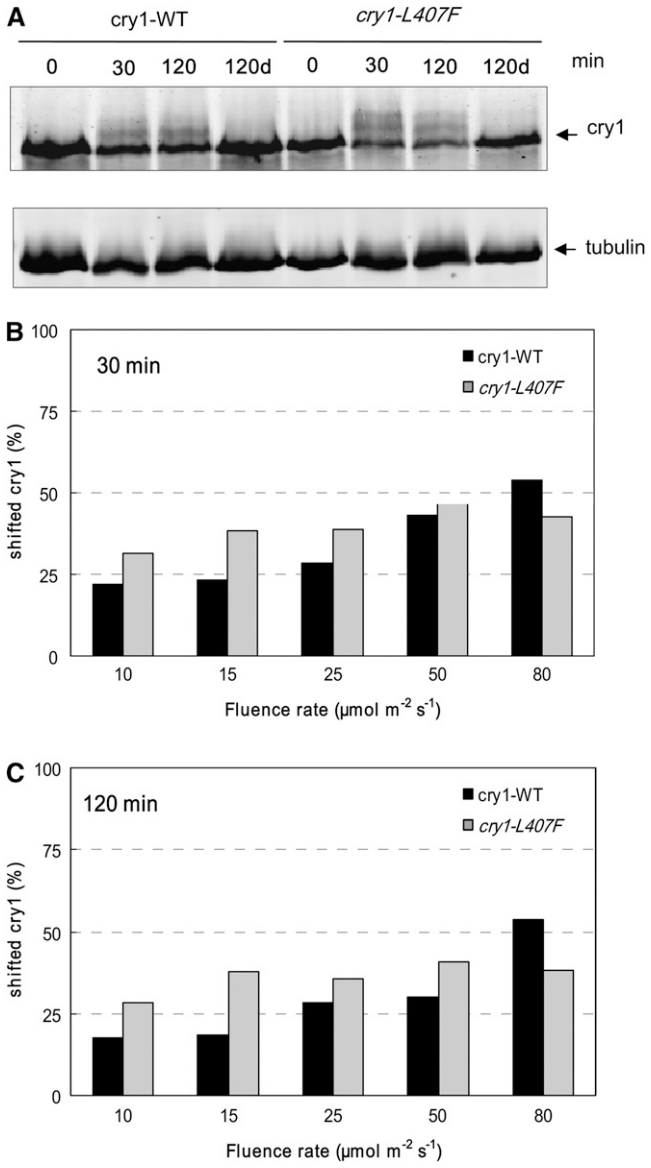

Figure 7. cry1-L407F is stronger phosphorylated in blue light than in wild-type cry1. Immunoblot analysis of wild-type cry1 (cry1-WT) and cry1-L407F protein levels (both in the *msi1-tap1* background). Seedlings were grown for 96 h in complete darkness before being transferred to monochromatic blue light (λ_{max} = 471 nm) of given fluence rates. A, Representative immunoblot of samples kept in darkness for 96 h (0), then irradiated with blue light for 30 or 120 min, or kept in darkness for another 120 min (120d). The blot shows samples from irradiation with 25 μmol m^{-2} s^{-1} blue light. The cry1 and tubulin signals are indicated with arrows. Note the shifted cry1 bands appearing in the light-treated samples that correspond to phosphorylated forms of cry1. B, Ratios of shifted (phosphorylated) cry1 to the total amount of cry1 in the respective genotypes. Seedlings were irradiated with the given fluence rates of blue light for 30 min. C, Same as B but seedlings were treated for 120 min with blue light. Quantification of the bands was done with the LI-COR Odyssey infrared imaging system and software in the linear range of cry1 and tubulin signals.

stable in all the simulated systems (RMSD = 2–3 Å). Generally, simulated RMSD were smaller for proteins with ATP than for proteins without ATP (Supplemental Fig. S4A). Interestingly, the crystallographic ATP-binding mode was unstable in the simulations of both wild-type and mutant proteins (Supplemental Fig. S5). During the simulations of the wild-type and mutated proteins, the distance between the N6 atom of ATP and the Cγ of Asp-409 was higher than the crystallographic distance of 3.5 Å (Supplemental Fig. S4B, top), indicating that this interaction is not maintained. Similarly, the RMSD plots of the adenine moiety of ATP showed instability of the ATP-binding mode in the wild-type and mutant proteins (Supplemental Fig. S4B, bottom; RMSD $>$ 5 Å). To identify potential regions of altered structural flexibility, we plotted root mean square fluctuation (RMSF) values of Cα atoms, which illustrate structural plasticity along the protein sequence. The RMSF plots of the wild-type protein show that ATP reduces the atomic fluctuations of three segments (Fig. 8A, top). The segments 1, 2, and 3 are spatially close to FAD and the adenine moiety of ATP, respectively (Fig. 1, left) but distant in sequence. A qualitative representation of the backbone flexibility where the thickness of the backbone is proportional to the RMSF is shown in Figure 8B. The RMSF plots of the mutant protein show that ATP reduces the atomic fluctuations only of segment 1, because the L407F mutation already has a stabilizing influence on segments 2 and 3 (Fig. 8A). To assess the effect of the mutation on the protein backbone flexibility, the residue-wise RMSF difference between the wild-type and mutant simulations without ATP was calculated (Fig. 8A, bottom). The 20 residues affected by the highest flexibility reduction include the mutation site; they are located in segments 2 and 3 and are close to the three conserved Trp residues (Fig. 1C, right).

Together, the simulations indicate that ATP binding stabilizes three regions of wild-type cry1 and that the L407F mutation partially mimics the effect of ATP binding by stabilizing two of three ATP binding-responsive regions even in the absence of ATP. Therefore, the differences in flexibility suggest that the L407F mutation reduces the conformational entropy penalty of ATP binding and thus might promote ATP binding, autophosphorylation, and eventually cry1 signaling.

DISCUSSION

cry1 Controls Flowering Time

Blue light promotes flowering (Guo et al., 1998), and this effect was attributed mainly to cry2, as *cry2* mutations delay flowering under LD conditions in a phyB-dependent manner (Koornneef et al., 1991; Guo et al., 1998, 1999; El-Din El-Assal et al., 2001, 2003; Endo et al., 2007; Liu et al., 2008b). Some studies had reported that cry1 functions in flowering time regulation as well, but others failed to find such evidence (Bagnall et al., 1996; Zagotta et al., 1996; Mockler et al., 1999; Blázquez et al., 2003). While *cry2* mainly affects flowering time under LD conditions, the effects on flowering time reported for certain cry1 alleles and the C-terminal domain of cry1 were prominent under SD conditions (Bagnall et al., 1996; Yang et al., 2000). Since both cry1 and cry2 are involved in blue light-mediated repression of hypocotyl elongation (Ahmad and Cashmore, 1993; Lin et al., 1998), it is also possible that both act to some extent in flowering time control but that the effect of cry1 on flowering time control is often masked by other floral regulators. In fact, it was reported that *cry1 cry2* double mutants flower significantly later than *cry2* single mutants when grown under monochromatic blue light (Mockler et al., 2003). Here, we describe the new *CRY1* allele *cry1-L407F*, which supports previous findings showing that cry1 can act as a positive regulator of the floral transition.

The *cry1-L407F* allele was isolated in a mutant screen for suppression of the late-flowering phenotype of *msi1-tap1* plants. Because *cry1-L407F* and *msi1-tap1* showed an additive genetic interaction (Supplemental Fig. S1), *MSI1* and *CRY1* possibly function in independent genetic pathways of flower induction.

cry1-L407F Causes Increased Expression of *CO* and *FT*

The cry1-L407F photoreceptor caused increased expression of *FT* (Fig. 3), and this can explain the observed early-flowering phenotype. *FT* plays only a minor role in flowering time regulation under SD, but high levels of *FT* expression cause early flowering even in SD. *FT* expression is affected by light in several ways. First, light controls the phase of the circadian clock to establish the correct diurnal expression of *CO*. Second, light stabilizes CO and allows the accumulation of CO specifically under LD, when expression peak and light coincide. This coincidence of the diurnal *CO* expression peak and external light stimulus is the main mechanism of photoperiodic acceleration of flowering by LD in Arabidopsis (Kobayashi and Weigel, 2007). Cryptochromes appear to play a dominant role in this process because they were proposed to be needed for CO degradation by CONSTITUTIVE PHOTOMORPHOGENIC1 (COP1) in the dark under SD (Jang et al., 2008; Liu et al., 2008b). Third, cry2 can also directly induce *FT* expression (Liu et al., 2008a).

Because increased *FT* expression in *cry1-L407F* remained constrained to the light period, it is unlikely that stabilization of CO by cry1-L407F in the dark caused the increased *FT* expression. In contrast, loss of COP1 leads to the stabilization of CO in the dark (Jang et al., 2008; Liu et al., 2008b) and to an *FT* transcript peak in the middle of the night (Jang et al., 2008). In *cry1-L407F*, *FT* expression peaked during the light period and was similarly low as in the wild type during the dark period, suggesting that cry1-L407F does not interfere with the degradation of CO protein by the COP1 pathway. In *cry1-L407F*, the increased *FT* expression during the light period is probably caused

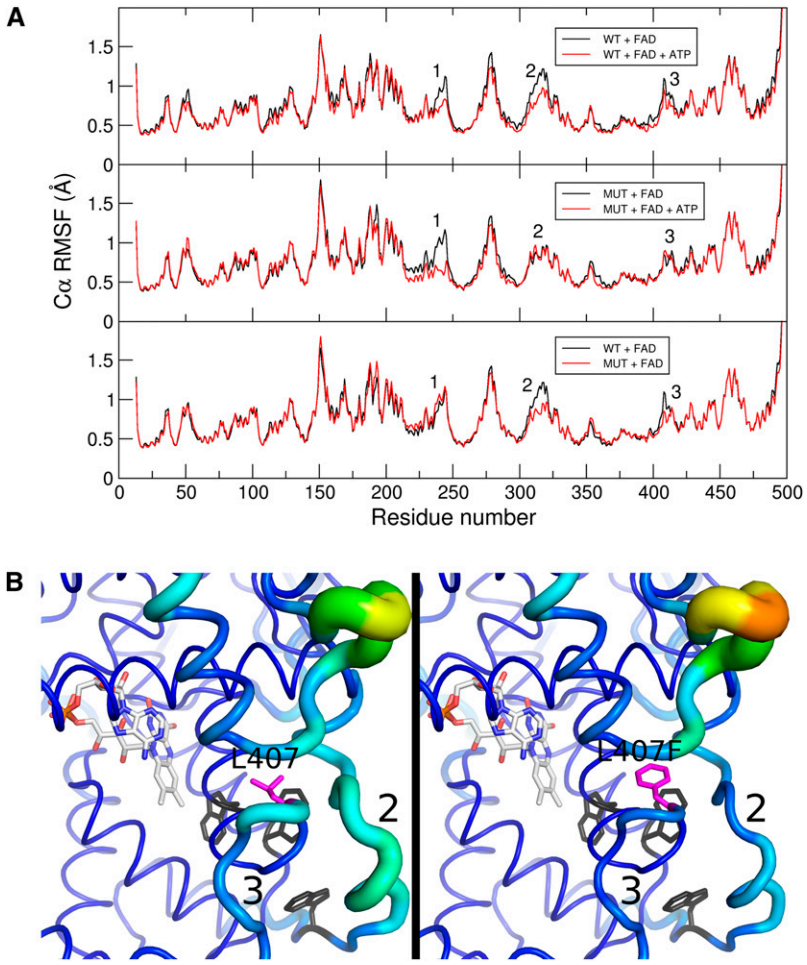

Figure 8. The L407F mutation reduces the structural flexibility of cry1. A, Comparison of backbone flexibility. Each curve is the average of the RMSF calculated over three trajectories. The segments corresponding to the peaks labeled 1, 2, and 3 are shown in Figure 1. WT, Wild type. B, The tube-like rendering of the backbone flexibility of the wild type (left) and cry1-L407F (right) was generated using values from A.

by the expression of *CO* during the light period. It is not clear how cry1-L407F caused increased *CO* expression during the light period. An indirect effect via altered function of the circadian clock seems unlikely given the unchanged expression of *ELF4* and *GI* (Fig. 3). It is conceivable, however, that cry1-L407F directly affects *CO* expression, a possibility we are currently testing.

A Conserved Leu Is Important for cry1 Function

Cryptochromes are flavoproteins with two chromophores and high sequence similarity to photolyases. However, cryptochromes lack several of the characteristics of the DNA-repairing photolyases, most prominently binding to DNA, which is explained by a negative electrostatic potential of the surface around the flavin-binding pocket of DNA-photolyase (Brautigam et al., 2004; Mees et al., 2004). In addition to the N-terminal photolyase-like PHR domain, cryptochromes contain a characteristic C-terminal domain, termed CCT, which is not present in the photolyases. Expression of the CCT domain in transgenic Arabidopsis led to constitutive photomorphogenesis and mimicked the phenotype of mutations in *COP1* (Yang et al., 2000). COP1 is involved in the regulation of hypocotyl elongation, anthocyanin production, and chloroplast development and binds to cry1 and cry2 via their CCT domains independent of light (Yang et al., 2000; Wang et al., 2001). It is possible that normally the CCT domain is kept inactive by an interaction with the PHR domain. Absorption of light would then cause conformational changes of the PHR domain, leading to release of the CCT domain, which could eventually activate the signaling chain (for review, see Lin and Todo, 2005). Because cry1 functions at least partially by affecting the ability of COP1 to ubiquitinate target proteins, which will then be degraded by the proteasome (Wang et al., 2001; Yang et al., 2001; Jang et al., 2008; Liu et al., 2008b; Kang et al., 2009), it is possible that cry1-L407F attenuates COP1 activity. This would lead to increased accumulation of HY5, causing light hypersensitivity of seedlings.

In addition to increased light sensitivity, the *cry1-L407F* mutants have some defects in skotomorphogenesis: cotyledons partially unfold, hypocotyls elongate less, and the light-induced *ELIP2* gene has a slightly increased basal expression in extended darkness. It is possible that the observed hypocotyl bending of dark-grown *cry1-L407F* seedlings was caused by an autonomous activation of phototropism. Notably,

light-activated wild-type cryptochrome has been implicated in phototropism (Ahmad et al., 1998a; Lascève et al., 1999; Kang et al., 2008; Tsuchida-Mayama et al., 2010). Because the hypocotyl bending of *cry1-L407F* mutants was much weaker at elevated growth temperatures, it is possible that the interaction with a cry1 signaling partner in the dark was enabled by the L407F mutation at 21°C but was not stable enough to remain effective at 26°C. Because *cry1-L407F* mutants differ from the wild type also under light conditions that do not activate cry1 (i.e. darkness and red and far-red light), cry1-L407F can partially function without the blue light requirement that is typical for wild-type cryptochromes. Thus, Leu-407 of cry1 seems to be essential to lock the photoreceptor in an inactive form and to prevent precocious activation of signaling cascades.

Leu-407 is located in a region of the protein that is conserved in all plant crytochromes but not in photolyases or animal cryptochromes (Fig. 1). Despite the strong conservation of Leu-407, it is not immediately obvious why the change to Phe, which is of similar size and hydrophobicity like Leu, would increase the light sensitivity of cry1. The mutated Leu-407 is close to the phosphate residues of AMP-PNP, sticking out of the flavin-binding pocket in the cocrystal structure of cry1 with AMP-PNP (Brautigam et al., 2004). To test whether the L407F mutation could modulate the ATP binding to cry1, molecular dynamics simulations of cry1 wild type and the L407F mutant in complex with FAD and with or without ATP were run. ATP binding reduced the Cα flexibility of three sequence segments, which are distant in sequence (segments 1 and 2, more than 50 amino acids; segments 2 and 3, more than 100 amino acids) but close in space. In contrast to the wild type, ATP binding did not reduce the flexibility of segments 2 and 3 in the L407F mutant because their flexibility is already diminished by the single point mutation.

To explain the hyperactivity of the *cry1-L407F* mutant, four not mutually exclusive hypotheses can be formulated. First, the novel Phe of the mutant is close to three conserved Trp residues, which are involved in electron transport from the surface to the FAD at least in vitro, as extensively studied in *Escherichia coli* photolyase, and considered to have the same function in plant cryptochromes (Park et al., 1995; Giovani et al., 2003; Banerjee et al., 2007). Thus, it is possible that cry1-L407F has altered photochemical properties. Second, partial prestabilization of the ATP-binding pocket in cry1-L407F could stabilize ATP binding, extending the lifetime of the signaling state of cry1. This conclusion is at least consistent with the increased level of shifted and phosphorylated cry1-L407F compared with wild-type cry1 (Fig. 7). Third, the reduced flexibility of cry1-L407F could favor binding to a signaling partner, because of a reduced conformational entropy penalty upon binding. Such an effect was recently observed for a mutant of a PDZ domain (Petit et al., 2009). Fourth, it is possible that conformational changes at the surface of cry1 induced by the L407F mutation altered cry1 binding specificity and led to the activation of signaling events that normally are not under cry1 control. The increased germination frequency of *cry1-L407F* mutants, for instance, could be explained by cry1-L407F having acquired a novel function in the control of germination, which is usually restricted to phytochromes. Discrimination between these possibilities will be addressed in future studies.

It is possible that the L407F exchange affects binding to interacting proteins. The fact that Leu-407 is in the N-terminal domain of cry1 suggests that partner recognition occurs, at least in part, via the N-terminal domain of cry and not exclusively via the C-terminal tail. The L407F exchange may be the first identified mutation that alters the downstream target specificity or affinity of cry.

Hypersensitivity of *cry1-L407F* to Various Light Qualities Reveals Tight Integration of Several Light Signaling Pathways

The *cry1-L407F* allele was not only hypersensitive to blue light but also to red and far-red light. Normally, red and far red light are not sensed by cryptochromes but by phytochromes. This raises the question of which photoreceptor is then responsible for the increased sensitivity to red light. Because the hypersensitivity of *cry1-L407F* to red pulses could be fully reverted by far-red pulses, at least in this case it was clearly phytochrome signaling that was affected in the *cry1-L407F* mutant. Interactions of red light-absorbing phytochrome and blue light-absorbing cryptochrome signaling cascades have been reported (Casal and Boccalandro, 1995; Ahmad and Cashmore, 1997; Hennig et al., 1999). Furthermore, nuclear import of phyB was initiated by blue light, but not by light of 695 nm, which establishes a similar phytochrome photoequilibrium as blue light (Gil et al., 2000). Finally, cryptochromes were found to be required for phytochrome signaling to the circadian clock (Devlin and Kay, 2000). On the molecular level, these effects could potentially be based on an interaction of the cry1 C-terminal domain with phyA (Ahmad et al., 1998b) or of cry2 with phyB (Más et al., 2000). Further work will establish whether the L407F mutation in cry1 affects direct interactions with phytochrome or whether the photochemical properties of cry1-L407F are changed. We propose that the increased sensitivity of *cry1-L407F* plants to blue, red, and far-red light reveals the intimate cross talk between cryptochrome and phytochrome light signaling cascades, which has been suggested to be important for concerted plant development under natural light conditions (Casal, 2000).

MATERIALS AND METHODS

Plant Material and Growth Conditions

Seeds of Col and Landsberg *erecta* Arabidopsis (*Arabidopsis thaliana*) wild-type accessions were obtained from the Nottingham Arabidopsis Seed Stock

Centre. The line *msi1-tap1* (accession Col) has been described before (Bouveret et al., 2006). The EMS allele *cry1-L407F* (accession Col) was isolated from a mutant screen (this study). To construct plants that ectopically overexpress cry1 or cry1-L407F (*35S::CRY1* and *35S::CRY1-L407F*), the full-length coding sequences were inserted into the binary destination vector pK7WG2 (Karimi et al., 2002) downstream of the cauliflower mosaic virus 35S promoter. Constructs were transformed into Col wild-type plants.

Seeds were usually germinated on sterile basal salts Murashige and Skoog medium (Duchefa) after 2 or 3 d of stratification treatment of the imbibed seeds at 4°C, and plants were analyzed on plates or transferred to soil (Einheitserde; H. Gilgen Optima-Werke) 10 d after germination. Alternatively, seeds were directly sown on soil. Plants were kept in Conviron growth chambers with mixed cold fluorescent and incandescent light (110–140 μmol m^{-2} s^{-1}, 21°C ± 2°C) under LD (16 h of light) or SD (8 h of light) photoperiods or were alternatively raised in greenhouses (LD, 14 h of light, 19°C/10 h of dark, 14°C; SD, 8 h of light, 20°C/16 h of dark, 20°C); if necessary, daylight was supplemented with mercury vapor lamps (Sylvania Lighting) to a maximum of 150 μmol m^{-2} s^{-1}.

For immunoblot analyses, seeds were plated on half-strength Murashige and Skoog plates and stratified at 4°C for 4 d in darkness. Germination was induced by white light illumination for 4 h. Plants were grown at 22°C for 4 d, and seedlings were harvested after treatment with blue light emitted from light-emitting diodes (λ_{max} = 471 nm; CLF Plant Climatics) for 30 or 120 min with the fluence rates indicated and measured with a P-2000 optometer (Gigahertz-Optik).

Flowering Time Analysis

Flowering time was scored as the length of time between the end of stratification and the development of a primary shoot of 5 mm height (=bolting). The number of rosette leaves was determined at bolting. For phase transition, all formed rosette leaves were inspected for the presence of abaxial trichomes at bolting.

RNA Isolation, Reverse Transcription-PCR, and Quantitative PCR

RNA was extracted from plant tissue as described previously (Hennig et al., 2003). For reverse transcription (RT)-PCR analysis, 1 μg of total RNA was treated with DNase I (Promega). The DNA-free RNA was reverse transcribed using a RevertAid First-Strand cDNA Synthesis Kit (Fermentas) according to the manufacturer's instructions. For quantitative PCR analysis, the Universal ProbeLibrary system (Roche Diagnostics) was used on a 7500 Fast Real-Time PCR instrument (Applied Biosystems). Quantitative PCR was performed with three replicates, and the results were analyzed as described (Exner et al., 2009). Details of the assays used are given in Supplemental Table S2.

Analysis of Hypocotyl Length

Seeds were plated on two layers of water-soaked 3MM chromatography paper (Whatman Schleicher & Schuell), which were placed into clear plastic boxes. A 48- to 96-h dark treatment at 4°C was followed by induction of germination by white light for 10 h (24 h for far-red studies) at 23°C and further incubation of the seedlings under specific light conditions, which were as follows: blue light, Philips TLD 18W/18 Blue E003, continuous light, 21°C; red light, Philips TLD 18W/18 Red, continuous light, 21°C; far-red light, as described (Sperling et al., 1997), continuous light, 26°C. The hypocotyl length was measured by spreading the seedlings on millimeter paper and reading the length.

Quantitative Immunoblots

Per sample, approximately 50 seedlings were collected, frozen in liquid nitrogen, and ground to a fine powder with a cell mill (MM200; Retsch). Protein was extracted by TCA-acetone precipitation according to Shultz et al. (2005) with the following modifications: after the washing steps, samples were dried in a SpeedVac and then dissolved in SDS sample buffer (45 mM Tris-HCl, pH 6.8, 10% glycerol, 1% SDS, 0.01% bromphenol blue, and 50 mM dithiothreitol). Samples were incubated at 95°C for 10 min followed by a centrifugation step (10 min, 20,000*g*) to remove cell debris. For SDS-PAGE, 15 μg of total protein was loaded per lane on 10% SDS minigels (Shultz et al., 2005). PageRuler (Fermentas) was used as marker. Separated proteins were transferred to nitrocellulose membranes (porablot NCP; Macherey-Nagel). Membranes were blocked with 7% milk powder in Tris-buffered saline (TBS; 20 mM Tris-HCl, pH 7.5, and 150 mM NaCl). Incubation with the two primary antibodies was done step-wise with monoclonal antibody against α-tubulin (anti-α-tubulin, produced in mouse; clone B-5-1-2; Sigma) and then with anti-cry1 antibody (raised in rabbits and provided by M. Ahmad, Universite Paris VI). Both antibodies were used in a 1:2,000 dilution in TBS-T (TBS with 0.1% [v/v] Tween 20). Fluorescence-labeled secondary antibodies against rabbit (donkey anti-rabbit IRDye800CW; LI-COR Biosciences) and mouse (donkey anti-mouse IRDye 700DX; Rockland) were incubated simultaneously for 1 h (each diluted 1:10,000 in TBS-T). The membranes were scanned and analyzed with the LI-COR Odyssey Infrared Imaging System. Bands detected in the 700-nm channel correspond to α-tubulin, and bands detected in the 800-nm channel correspond to cry1. The system was calibrated to ensure measurements in the linear range for both α-tubulin and cry1. The cry1 signal was normalized against the α-tubulin signal. In addition, the percentage of shifted cry1 bands compared with the total cry1 signal was determined.

Sequence Alignment

The Arabidopsis CRY1 (At4g08920), CRY2 (At1g04400), and photolyase (At3g15620) protein sequences were obtained from The Arabidopsis Information Resource (http://www.arabidopsis.org/) and blasted against the nonredundant protein databases at the National Center for Biotechnology Information (http://www.ncbi.nlm.nih.gov/sites/entrez?cmd=Search&db=pubmed) and at the Department of Energy Joint Genome Institute (http://genome.jgi-psf.org/). The obtained sequences were aligned using ClustalX 2.0. The identifiers of the protein sequences included in this analysis are listed in Supplemental Table S3. The nomenclature of phytochrome as well as cryptochrome photoreceptors and their genes is according to Quail et al. (1994).

Molecular Dynamics Simulations

The crystal structure of the PHR domain of Arabidopsis cry1 with AMP-PNP bound (Protein Data Bank accession code 1U3D) was used for modeling and molecular dynamics simulations. The L407F mutation was introduced with PyMOL (The PyMOL Molecular Graphics System, version 1.2r1; Schrödinger), and the most common rotamer was selected. To generate ATP from AMP-PNP, the nitrogen atom between phosphate groups of AMP-PNP was replaced by oxygen. Ions and crystallization water were kept for further calculations. All the simulations were carried out using CHARMM version c35b2 (Brooks et al., 1983, 2009) and the PARAM22 force field (Mackerell et al., 1998, 2004) with the TIP3P model of water (Jorgensen et al., 1983; Mackerell et al., 1998). To effectively compare simulations with experiments, pH 7.4 was considered. The side chains of Asp and Glu residues were negatively charged, those of Lys and Arg residues were positively charged, His residues were considered neutral, the N terminus was positively charged, and the C terminus was negatively charged. First, structures were minimized in vacuo using a dielectric constant $\varepsilon = 4r$ (where r is the distance in Å between atoms/partial charges) to an energy gradient of 0.01 kcal mol^{-1} $Å^{-1}$. The minimized protein was then inserted into a water box, where each atom of the protein had a distance of at least 14 Å from the boundary. Water molecules within 2.8 Å from any atom of the protein were removed. Chloride and sodium ions were added to neutralize the total charge of the system at a concentration of 200 mM. The final system consisted of around 96,000 atoms, approximately 7,900 of which belong to the solute. To avoid finite-size effects, periodic boundary conditions were applied. Long-range electrostatic effects were taken into account by the Particle Mesh Ewald summation method (Darden et al., 1993). The temperature was kept constant at 300 K by the Nosé-Hoover thermostat (Nose, 1984; Hoover, 1985), while the pressure was held constant at 1 atm by applying the Langevin piston pressostat. Lookup tables (Nilsson, 2009) for the calculation of water-water nonbonded interactions (van der Waals and Coulomb) were used to increase efficiency. SHAKE was applied to the hydrogens, allowing an integration step of 2 fs. Different initial random velocities were assigned to every simulation. Four systems were simulated: the wild-type protein with only FAD bound; the wild-type protein with FAD and ATP bound; the mutant with only FAD bound; and the mutant with FAD and ATP bound. Three independent 30-ns-long simulations were carried out for each system.

Trajectory Analyses

RMSD and RMSF were calculated with CHARMM, and their formulae are as follows:

$$\mathrm{RMSD} = \sqrt{\frac{1}{N}\sum_{i=1}^{N}(x_i - x_{i,\mathrm{ref}})^2 + \left(y_i - y_{i,\mathrm{ref}}\right)^2 + (z_i - z_{i,\mathrm{ref}})^2}$$

$$\mathrm{RMSF}_i = \sqrt{\frac{1}{N_f}\sum_{i=1}^{N_f}(x_i - x_{i,\mathrm{ave}})^2 + \left(y_i - y_{i,\mathrm{ave}}\right)^2 + (z_i - z_{i,\mathrm{ave}})^2}$$

where N is the number of atoms; x_i, y_i, and z_i are the coordinates of the atom i after best superposition on a reference structure; and $x_{i,\mathrm{ref}}$, $y_{i,\mathrm{ref}}$, and $z_{i,\mathrm{ref}}$ are the coordinates of the atom i in the reference structure. The coordinates x_i, y_i, and z_i refer to the average structure; N_f is the number of frames in the trajectory segment analyzed for RMSF calculations; the coordinates $x_{i,\mathrm{ave}}$, $y_{i,\mathrm{ave}}$, and $z_{i,\mathrm{ave}}$ refer to the average structure. The reference structure for RMSD analyses was the starting structure used in the dynamics (i.e. the energy-minimized x-ray structure). The average structures and RMSF were calculated along 2-ns segments of trajectory, skipping the first 2 ns and the last incomplete segment shorter than 2 ns. For the first 30 ns of simulation time, 13 values of RMSF were calculated and then averaged. RMSD expresses how different an object is with respect to another after the best superposition of the two. A RMSD value of zero means perfect superposition. RMSF is a measure of atomic flexibility and can be related to the crystallographic B-factor, $B = 8\pi^2/3(\mathrm{RMSF})^2$. The distance between the N6 atom of ATP and the Cγ of Asp-409 was calculated with the program Wordom (Seeber et al., 2007). Structures were plotted with PyMOL.

Supplemental Data

The following materials are available in the online version of this article.

Supplemental Figure S1. *cry1-L407F* and *msi1-tap1* affect flowering time additively.

Supplemental Figure S2. Emission spectrum of the red light source.

Supplemental Figure S3. Phenotype of *cry1-L407F* seedlings in the dark.

Supplemental Figure S4. Structural stability of the PHR domain of cry1 and stability of the ATP-binding mode.

Supplemental Figure S5. Binding mode displacement of ATP.

Supplemental Table S1. Phenotype of *cry1-L407F* seedlings in the dark.

Supplemental Table S2. Primers used for quantitative RT-PCR.

Supplemental Table S3. Protein sequences used for the alignment.

ACKNOWLEDGMENT

We thank Romaric Bouveret for help during the EMS treatment of *msi1-tap1* seeds.

Received June 15, 2010; accepted October 5, 2010; published October 6, 2010.

LITERATURE CITED

Ahmad M, Cashmore AR (1993) HY4 gene of A. thaliana encodes a protein with characteristics of a blue-light photoreceptor. Nature **366:** 162–166

Ahmad M, Cashmore AR (1997) The blue-light receptor cryptochrome 1 shows functional dependence on phytochrome A or phytochrome B in *Arabidopsis thaliana*. Plant J **11:** 421–427

Ahmad M, Grancher N, Heil M, Black RC, Giovani B, Galland P, Lardemer D (2002) Action spectrum for cryptochrome-dependent hypocotyl growth inhibition in Arabidopsis. Plant Physiol **129:** 774–785

Ahmad M, Jarillo JA, Smirnova O, Cashmore AR (1998a) Cryptochrome blue-light photoreceptors of Arabidopsis implicated in phototropism. Nature **392:** 720–723

Ahmad M, Jarillo JA, Smirnova O, Cashmore AR (1998b) The CRY1 blue light photoreceptor of Arabidopsis interacts with phytochrome A in vitro. Mol Cell **1:** 939–948

Bagnall DJ, King RW, Hangarter RP (1996) Blue-light promotion of flowering is absent in *hy4* mutants of Arabidopsis. Planta **200:** 278–280

Banerjee R, Batschauer A (2005) Plant blue-light receptors. Planta **220:** 498–502

Banerjee R, Schleicher E, Meier S, Viana RM, Pokorny R, Ahmad M, Bittl R, Batschauer A (2007) The signaling state of Arabidopsis cryptochrome 2 contains flavin semiquinone. J Biol Chem **282:** 14916–14922

Blázquez MA, Ahn JH, Weigel D (2003) A thermosensory pathway controlling flowering time in *Arabidopsis thaliana*. Nat Genet **33:** 168–171

Bouly JP, Giovani B, Djamei A, Mueller M, Zeugner A, Dudkin EA, Batschauer A, Ahmad M (2003) Novel ATP-binding and autophosphorylation activity associated with Arabidopsis and human cryptochrome-1. Eur J Biochem **270:** 2921–2928

Bouveret R, Schönrock N, Gruissem W, Hennig L (2006) Regulation of flowering time by Arabidopsis MSI1. Development **133:** 1693–1702

Brautigam CA, Smith BS, Ma Z, Palnitkar M, Tomchick DR, Machius M, Deisenhofer J (2004) Structure of the photolyase-like domain of cryptochrome 1 from *Arabidopsis thaliana*. Proc Natl Acad Sci USA **101:** 12142–12147

Brooks BR, Brooks CL III, Mackerell AD Jr, Nilsson L, Petrella RJ, Roux B, Won Y, Archontis G, Bartels C, Boresch S, et al (2009) CHARMM: the biomolecular simulation program. J Comput Chem **30:** 1545–1614

Brooks BR, Bruccoleri RE, Olafson BD, States DJ, Swaminathan S, Karplus M (1983) CHARMM: a program for macromolecular energy, minimization, and dynamics calculations. J Comput Chem **4:** 187–217

Casal JJ (2000) Phytochromes, cryptochromes, phototropin: photoreceptor interactions in plants. Photochem Photobiol **71:** 1–11

Casal JJ, Boccalandro H (1995) Co-action between phytochrome B and HY4 in *Arabidopsis thaliana*. Planta **197:** 213–218

Casal JJ, Mazzella MA (1998) Conditional synergism between cryptochrome 1 and phytochrome B is shown by the analysis of *phyA*, *phyB*, and *hy4* simple, double, and triple mutants in Arabidopsis. Plant Physiol **118:** 19–25

Darden T, York D, Pedersen L (1993) An N· log (N) method for Ewald sums in large systems. J Chem Phys **98:** 10089–10092

Devlin PF, Kay SA (2000) Cryptochromes are required for phytochrome signaling to the circadian clock but not for rhythmicity. Plant Cell **12:** 2499–2510

Doyle MR, Davis SJ, Bastow RM, McWatters HG, Kozma-Bognár L, Nagy F, Millar AJ, Amasino RM (2002) The *ELF4* gene controls circadian rhythms and flowering time in *Arabidopsis thaliana*. Nature **419:** 74–77

El-Din El-Assal S, Alonso-Blanco C, Peeters AJ, Raz V, Koornneef M (2001) A QTL for flowering time in Arabidopsis reveals a novel allele of CRY2. Nat Genet **29:** 435–440

El-Din El-Assal S, Alonso-Blanco C, Peeters AJ, Wagemaker C, Weller JL, Koornneef M (2003) The role of cryptochrome 2 in flowering in Arabidopsis. Plant Physiol **133:** 1504–1516

Endo M, Mochizuki N, Suzuki T, Nagatani A (2007) CRYPTOCHROME2 in vascular bundles regulates flowering in *Arabidopsis*. Plant Cell **19:** 84–93

Exner V, Aichinger E, Shu H, Wildhaber T, Alfarano P, Caflisch A, Gruissem W, Köhler C, Hennig L (2009) The chromodomain of LIKE HETEROCHROMATIN PROTEIN 1 is essential for H3K27me3 binding and function during Arabidopsis development. PLoS ONE **4:** e5335

Franklin KA, Larner VS, Whitelam GC (2005) The signal transducing photoreceptors of plants. Int J Dev Biol **49:** 653–664

Gil P, Kircher S, Adam E, Bury E, Kozma-Bognar L, Schäfer E, Nagy F (2000) Photocontrol of subcellular partitioning of phytochrome-B:GFP fusion protein in tobacco seedlings. Plant J **22:** 135–145

Giovani B, Byrdin M, Ahmad M, Brettel K (2003) Light-induced electron transfer in a cryptochrome blue-light photoreceptor. Nat Struct Biol **10:** 489–490

Guo H, Duong H, Ma N, Lin C (1999) The Arabidopsis blue light receptor cryptochrome 2 is a nuclear protein regulated by a blue light-dependent post-transcriptional mechanism. Plant J **19:** 279–287

Guo HW, Yang H, Mockler TC, Lin CT (1998) Regulation of flowering time by Arabidopsis photoreceptors. Science **279:** 1360–1363

Harari-Steinberg O, Ohad I, Chamovitz DA (2001) Dissection of the light signal transduction pathways regulating the two early light-induced protein genes in Arabidopsis. Plant Physiol **127:** 986–997

Hennig L, Funk M, Whitelam GC, Schäfer E (1999) Functional interaction of cryptochrome 1 and phytochrome D. Plant J **20:** 289–294

Hennig L, Taranto P, Walser M, Schönrock N, Gruissem W (2003) Arabidopsis MSI1 is required for epigenetic maintenance of reproductive development. Development **130:** 2555–2565

Hoover WG (1985) Canonical dynamics: equilibrium phase-space distributions. Phys Rev A **31:** 1695–1697

Jang S, Marchal V, Panigrahi KC, Wenkel S, Soppe W, Deng XW, Valverde F, Coupland G (2008) Arabidopsis COP1 shapes the temporal pattern of CO accumulation conferring a photoperiodic flowering response. EMBO J **27:** 1277–1288

Johnson E, Bradley M, Harberd NP, Whitelam GC (1994) Photoresponses of light-grown *phyA* mutants of Arabidopsis. Plant Physiol **105:** 141–149

Jorgensen WL, Chandrasekhar J, Madura JD, Impey RW, Klein MK (1983) Comparison of simple potential functions for simulating liquid water. J Chem Phys **79:** 926–935

Josse EM, Foreman J, Halliday KJ (2008) Paths through the phytochrome network. Plant Cell Environ **31:** 667–678

Kang B, Grancher N, Koyffmann V, Lardemer D, Burney S, Ahmad M (2008) Multiple interactions between cryptochrome and phototropin blue-light signalling pathways in *Arabidopsis thaliana*. Planta **227:** 1091–1099

Kang CY, Lian HL, Wang FF, Huang JR, Yang HQ (2009) Cryptochromes, phytochromes, and COP1 regulate light-controlled stomatal development in *Arabidopsis*. Plant Cell **21:** 2624–2641

Karimi M, Inzé D, Depicker A (2002) Gateway vectors for Agrobacterium-mediated plant transformation. Trends Plant Sci **7:** 193–195

Kobayashi Y, Weigel D (2007) Move on up, it's time for change: mobile signals controlling photoperiod-dependent flowering. Genes Dev **21:** 2371–2384

Koornneef M, Hanhart CJ, van der Veen JH (1991) A genetic and physiological analysis of late flowering mutants in *Arabidopsis thaliana*. Mol Gen Genet **229:** 57–66

Koornneef M, Rolff E, Spruit CJP (1980) Genetic control of light-inhibited hypocotyl elongation in *Arabidopsis thaliana.* Z Pflanzenphysiol **100:** 147–160

Lascève G, Leymarie J, Olney MA, Liscum E, Christie JM, Vavasseur A, Briggs WR (1999) Arabidopsis contains at least four independent blue-light-activated signal transduction pathways. Plant Physiol **120:** 605–614

Lin C, Ahmad M, Gordon D, Cashmore AR (1995) Expression of an Arabidopsis cryptochrome gene in transgenic tobacco results in hypersensitivity to blue, UV-A, and green light. Proc Natl Acad Sci USA **92:** 8423–8427

Lin C, Todo T (2005) The cryptochromes. Genome Biol **6:** 220

Lin CT, Ahmad M, Cashmore AR (1996) Arabidopsis cryptochrome 1 is a soluble protein mediating blue light-dependent regulation of plant growth and development. Plant J **10:** 893–902

Lin CT, Yang HY, Guo HW, Mockler T, Chen J, Cashmore AR (1998) Enhancement of blue-light sensitivity of Arabidopsis seedlings by a blue light receptor cryptochrome 2. Proc Natl Acad Sci USA **95:** 2686–2690

Liu H, Yu X, Li K, Klejnot J, Yang H, Lisiero D, Lin C (2008a) Photoexcited CRY2 interacts with CIB1 to regulate transcription and floral initiation in Arabidopsis. Science **322:** 1535–1539

Liu LJ, Zhang YC, Li QH, Sang Y, Mao J, Lian HL, Wang L, Yang HQ (2008b) COP1-mediated ubiquitination of CONSTANS is implicated in cryptochrome regulation of flowering in *Arabidopsis*. Plant Cell **20:** 292–306

Mackerell AD, Bashford D, Bellot M, Dunbrack RL, Evanseck DJ, Field MJ, Fischer S, Gao J, Guo H, Ha G, et al (1998) All-atom empirical potential for molecular modeling and dynamics studies of proteins. J Phys Chem B **102:** 3586–3616

Mackerell AD Jr, Feig M, Brooks CL III (2004) Extending the treatment of backbone energetics in protein force fields: limitations of gas-phase quantum mechanics in reproducing protein conformational distributions in molecular dynamics simulations. J Comput Chem **25:** 1400–1415

Más P, Devlin PF, Panda S, Kay SA (2000) Functional interaction of phytochrome B and cryptochrome 2. Nature **408:** 207–211

Mees A, Klar T, Gnau P, Hennecke U, Eker AP, Carell T, Essen LO (2004) Crystal structure of a photolyase bound to a CPD-like DNA lesion after in situ repair. Science **306:** 1789–1793

Mockler T, Yang H, Yu X, Parikh D, Cheng YC, Dolan S, Lin C (2003) Regulation of photoperiodic flowering by Arabidopsis photoreceptors. Proc Natl Acad Sci USA **100:** 2140–2145

Mockler TC, Guo HW, Yang HY, Duong H, Lin CT (1999) Antagonistic actions of Arabidopsis cryptochromes and phytochrome B in the regulation of floral induction. Development **126:** 2073–2082

Müller M, Carell T (2009) Structural biology of DNA photolyases and cryptochromes. Curr Opin Struct Biol **19:** 277–285

Neff MM, Chory J (1998) Genetic interactions between phytochrome A, phytochrome B, and cryptochrome 1 during Arabidopsis development. Plant Physiol **118:** 27–35

Nilsson L (2009) Efficient table lookup without inverse square roots for calculation of pair wise atomic interactions in classical simulations. J Comput Chem **30:** 1490–1498

Nose S (1984) A unified formulation of the constant temperature molecular dynamics methods. J Chem Phys **81:** 511–520

Oh E, Yamaguchi S, Hu J, Yusuke J, Jung B, Paik I, Lee HS, Sun TP, Kamiya Y, Choi G (2007) PIL5, a phytochrome-interacting bHLH protein, regulates gibberellin responsiveness by binding directly to the *GAI* and *RGA* promoters in *Arabidopsis* seeds. Plant Cell **19:** 1192–1208

Park DH, Somers DE, Kim YS, Choy YH, Lim HK, Soh MS, Kim HJ, Kay SA, Nam HG (1999) Control of circadian rhythms and photoperiodic flowering by the Arabidopsis *GIGANTEA* gene. Science **285:** 1579–1582

Park HW, Kim ST, Sancar A, Deisenhofer J (1995) Crystal structure of DNA photolyase from *Escherichia coli*. Science **268:** 1866–1872

Petit CM, Zhang J, Sapienza PJ, Fuentes EJ, Lee AL (2009) Hidden dynamic allostery in a PDZ domain. Proc Natl Acad Sci USA **106:** 18249–18254

Pokorny R, Klar T, Hennecke U, Carell T, Batschauer A, Essen LO (2008) Recognition and repair of UV lesions in loop structures of duplex DNA by DASH-type cryptochrome. Proc Natl Acad Sci USA **105:** 21023–21027

Quail PH, Briggs WR, Chory J, Hangarter RP, Harberd NP, Kendrick RE, Koornneef M, Parks B, Sharrock RA, Schäfer E, et al (1994) Spotlight on phytochrome nomenclature. Plant Cell **6:** 468–471

Reed JW, Nagatani A, Elich TD, Fagan M, Chory J (1994) Phytochrome A and phytochrome B have overlapping but distinct functions in Arabidopsis development. Plant Physiol **104:** 1139–1149

Reed JW, Nagpal P, Poole DS, Furuya M, Chory J (1993) Mutations in the gene for the red/far-red light receptor phytochrome B alter cell elongation and physiological responses throughout *Arabidopsis* development. Plant Cell **5:** 147–157

Seeber M, Cecchini M, Rao F, Settanni G, Caflisch A (2007) Wordom: a program for efficient analysis of molecular dynamics simulations. Bioinformatics **23:** 2625–2627

Selby CP, Sancar A (2006) A cryptochrome/photolyase class of enzymes with single-stranded DNA-specific photolyase activity. Proc Natl Acad Sci USA **103:** 17696–17700

Shalitin D, Yang H, Mockler TC, Maymon M, Guo H, Whitelam GC, Lin C (2002) Regulation of Arabidopsis cryptochrome 2 by blue-light-dependent phosphorylation. Nature **417:** 763–767

Shalitin D, Yu X, Maymon M, Mockler T, Lin C (2003) Blue light-dependent in vivo and in vitro phosphorylation of *Arabidopsis* cryptochrome 1. Plant Cell **15:** 2421–2429

Shinomura T, Nagatani A, Hanzawa H, Kubota M, Watanabe M, Furuya M (1996) Action spectra for phytochrome A- and B-specific photoinduction of seed germination in *Arabidopsis thaliana*. Proc Natl Acad Sci USA **93:** 8129–8133

Shultz RW, Settlage RE, Hanley-Bowdoin L, Thompson WF (2005) A trichloroacetic acid-acetone method greatly reduces infrared autofluorescence of protein extracts from plant tissue. Plant Mol Biol Rep **23:** 405–409

Sperling U, van Cleve B, Frick G, Apel K, Armstrong GA (1997) Overexpression of light-dependent PORA or PORB in plants depleted of endogenous POR by far-red light enhances seedling survival in white light and protects against photooxidative damage. Plant J **12:** 649–658

Tsuchida-Mayama T, Sakai T, Hanada A, Uehara Y, Asami T, Yamaguchi S (2010) Role of the phytochrome and cryptochrome signaling pathways in hypocotyl phototropism. Plant J **62:** 653–662

Wang H, Ma LG, Li JM, Zhao HY, Deng XW (2001) Direct interaction of Arabidopsis cryptochromes with COP1 in light control development. Science **294:** 154–158

Yang HQ, Tang RH, Cashmore AR (2001) The signaling mechanism of *Arabidopsis* CRY1 involves direct interaction with COP1. Plant Cell **13:** 2573–2587

Yang HQ, Wu YJ, Tang RH, Liu D, Liu Y, Cashmore AR (2000) The C termini of Arabidopsis cryptochromes mediate a constitutive light response. Cell **103:** 815–827

Yu X, Shalitin D, Liu X, Maymon M, Klejnot J, Yang H, Lopez J, Zhao X, Bendehakkalu KT, Lin C (2007) Derepression of the NC80 motif is critical for the photoactivation of Arabidopsis CRY2. Proc Natl Acad Sci USA **104:** 7289–7294

Zagotta MT, Hicks KA, Jacobs CI, Young JC, Hangarter RP, Meeks-Wagner DR (1996) The Arabidopsis *ELF3* gene regulates vegetative photomorphogenesis and the photoperiodic induction of flowering. Plant J **10:** 691–702